

A new quadruple gravitational lens from the Hyper Suprime-Cam Survey: the dilemma of HSC J115252+004733

Anupreeta More,^{1*} Chien-Hsiu Lee,² Masamune Oguri,^{1,3,4} Yoshiaki Ono,⁵ Sherry H. Suyu,^{6,7} James H. H. Chan,^{7,8} John D. Silverman,¹ Surhud More,¹ Andreas Schulze,¹ Yutaka Komiyama,^{9,10} Yoshiki Matsuoka,⁹ Satoshi Miyazaki,^{9,10} Tohru Nagao,¹¹ Masami Ouchi,⁵ Philip J. Tait,¹² Manobu M. Tanaka,¹³ Masayuki Tanaka,⁹ Tomonori Usuda^{9,10} and Naoki Yasuda¹

¹ Kavli Institute for the Physics and Mathematics of the Universe (Kavli IPMU, WPI), University of Tokyo, Chiba 277-8583, Japan

² Subaru Telescope, National Astronomical Observatory of Japan, 650 North Aohoku Place, Hilo, HI 96720, USA

³ Research Center for the Early Universe, University of Tokyo, 7-3-1 Hongo, Bunkyo-ku, Tokyo 113-0033, Japan

⁴ Department of Physics, University of Tokyo, 7-3-1 Hongo, Bunkyo-ku, Tokyo 113-0033, Japan

⁵ Institute for Cosmic Ray Research, The University of Tokyo, 5-1-5 Kashiwa-no-Ha, Kashiwa City, Chiba, 277-8582, Japan

⁶ Max-Planck-Institut für Astrophysik, Karl-Schwarzschild-Str. 1, 85748 Garching, Germany

⁷ Institute of Astronomy and Astrophysics, Academia Sinica, P.O. Box 23-141, Taipei 10617, Taiwan

⁸ Department of Physics, National Taiwan University, Taipei 10617, Taiwan

⁹ National Astronomical Observatory of Japan, 2-21-1 Osawa, Mitaka, Tokyo 181-8588, Japan

¹⁰ SOKENDAI (The Graduate University for Advanced Studies), Osawa, Mitaka, Tokyo 181-8588, Japan

¹¹ Research Center for Space and Cosmic Evolution, Ehime University, Bunkyo-cho 2-5, Matsuyama, Ehime 790-8577, Japan

¹² Subaru Telescope, 650 North Aohoku Place, Hilo, HI 96720, USA

¹³ High Energy Accelerator Research Organization, Institute of Particle and Nuclear Studies, KEK, 1-1 Oho, Tsukuba, Ibaraki 305-0801, Japan

25 October 2021

ABSTRACT

We report the serendipitous discovery of a quadruply (quad) lensed source at redshift $z_s = 3.76$, HSC J115252+004733, from the Subaru Hyper Suprime-Cam (HSC) Survey. The source is lensed by an early-type galaxy at $z_l = 0.466$ along with a satellite galaxy. Here, we investigate the nature of the source by studying its size, luminosity and from follow-up spectroscopy, the luminosity and velocity width of the Ly- α emission line. Our analyses suggest that the source is most probably a low-luminosity active galactic nucleus (AGN) or possibly an unusually compact and bright galaxy such as a Lyman- α emitter or a Lyman Break Galaxy. The morphology of the brighter pair of lensed images appears point-like except in the HSC i -band which was observed in better seeing conditions ($\sim 0''.5$). The extended feature in the i -band image can be explained by the emission from the host galaxy of the AGN, or alternatively, the highly compact lensed galaxy which appears point-like in all bands except in i -band. We also find that the flux ratio of the brighter pair of images show variation in the near-infrared compared to the optical imaging. Phenomena such as differential extinction and intrinsic variability cannot explain this chromatic variation. While microlensing from stars in the foreground galaxy is less likely to be the cause, it cannot be ruled out completely. If the galaxy hosts an AGN, then this represents the highest redshift quadruply imaged AGN known to date. Discovery of this unusually compact and faint source demonstrates the potential of the HSC survey.

Key words: gravitational lensing: strong – methods: observational – quasars: individual

1 INTRODUCTION

Gravitational lensing acts as a natural telescope to provide a sneak peek at some of the most distant and faintest galaxies and quasars in

* anupreeta.more@ipmu.jp

the Universe. Multiple, magnified images of these distant sources provide an unprecedented view into their properties. Gravitational lensing has thus been proven to be a powerful astrophysical and cosmological tool.

Populations of distant galaxy are mostly comprised of star-forming galaxies (SFGs) often identified in observations as Lyman Break Galaxies (LBGs) or Lyman- α emitters (LAEs). The magnification due to gravitational lensing is critical to study the faint end of the distant LAE and LBG populations at high angular resolution. Lensing has enabled several studies such as sources of cosmic reionization (e.g., Stark et al. 2007; Atek et al. 2015), understanding the physical properties of LAEs/LBGs at high redshifts $z = 6 - 7$ (e.g., Egami et al. 2005; Bradley et al. 2008; Huang et al. 2016), their molecular gas and inter-stellar medium (ISM) properties (e.g., Riechers et al. 2010; Rawle et al. 2014) as well as their abundances (e.g., Bradley et al. 2014; Schmidt et al. 2016).

Lensed quasars have also proven to be useful as both cosmological and astrophysical probes. For example, the time delays between the intensity variations in the quasar images, along with ancillary data to break the mass-sheet degeneracy (e.g., Falco et al. 1985; Schneider & Sluse 2013), provide a direct way to measure cosmological parameters (e.g., Refsdal 1964; Oguri 2007; Tewes et al. 2013; Suyu et al. 2013, 2014; Bonvin et al. 2016; Suyu et al. 2016; Wong et al. 2016). Flux ratio anomalies in lensed quasars have been used to constrain the fraction of dark matter substructure in the dark matter halos of lens galaxies (e.g., Dalal & Kochanek 2002; Nierenberg et al. 2014; Xu et al. 2015). The magnification of lensed quasars also allows a clearer view of the spatial structure of the line emitting region (e.g., Yonehara 2006), and diagnosis of their inner structure via microlensing (e.g., Morgan et al. 2008; Motta et al. 2012). Quasar microlensing also enables us to directly measure the fraction of mass in stars in the foreground lens at the position of the quasar images. This provides crucial information to measure the stellar initial mass function of lensing galaxies (e.g., Oguri et al. 2014; Schechter et al. 2014; Jiménez-Vicente et al. 2015). Furthermore, source reconstruction of lensed quasars and their host gives a direct view on the co-evolution of quasars and host galaxies up to $z \sim 4$ (e.g., Peng et al. 2002; Rusu et al. 2016).

Systematic searches for lensed quasars have successfully found over a hundred lens systems, in the radio (e.g., Myers et al. 2003; Browne et al. 2003), in the optical (e.g., Oguri et al. 2006; Inada et al. 2012; More et al. 2016) as well as other multi-wavelength regimes (e.g., Jackson et al. 2012). On galaxy scales, lensed quasars are typically doubly imaged (“doubles”) or quadruply imaged (“quads”). Most of the lensed quasar systems discovered to date are doubles. For example, a sample of thirteen lensed quasars recently discovered by More et al. (2016) from the Sloan Digital Sky Survey-III are all doubles. Nonetheless, quads with their two additional images provide additional astrophysical information on the foreground lens and the background source. Finding more quad quasar lenses is thus of tremendous value to the community given the small number¹ of currently known quads.

In this paper, we report the discovery of the quad lens HSC J115252+004733 (henceforth referred to as HSC J1152+0047) from the Hyper Suprime-Cam (HSC) Survey. The HSC Survey is a Subaru Strategic Program (SSP) using

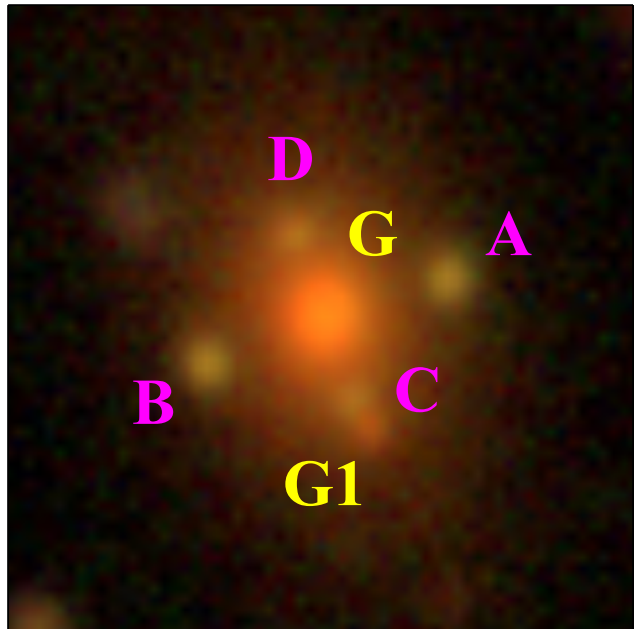


Figure 1. Color (*gri*) composite of HSC J1152+0047 showing the four blue lensed images (A, B, C and D) in an Einstein-cross configuration. Apart from the central lensing galaxy (G), a companion galaxy (G1, close to image C) is probably contributing to lensing. The image is 10'' on the side. North is up and East is left.

the newly installed HSC (Miyazaki et al. 2012) instrument on the Subaru 8.2-m telescope. The survey consists of three layers (wide, deep, ultradeep), where the wide layer is expected to cover $\sim 1400 \text{ deg}^2$ in *grizY*-bands down to a depth of $r \sim 26$. The HSC data are processed with *hscPipe*, which is derived from the LSST software pipeline (Ivezic et al. 2008; Axelrod et al. 2010; Jurić et al. 2015), and are calibrated using the Pan-STARRS1 data (Tonry et al. 2012; Schlafly et al. 2012; Magnier et al. 2013).

Our paper is organized as follows. In Section 2, we describe the discovery of HSC J1152+0047 and the multi-wavelength imaging data on this lens system. We describe the spectroscopic follow-up in Section 3. The lens mass modeling is described in Section 4. In Section 5, we derive the properties of the delensed source. In Section 6, we compare our source with other distant galaxies and quasars to understand its nature and discuss the cause of chromatic variation in flux ratios. We present our conclusions in Section 7. Magnitudes quoted in this paper are in AB magnitudes unless otherwise stated. We note that the terms active galactic nuclei (AGN) and quasar are used interchangeably in the text. We used the following cosmological parameters wherever necessary $\Omega_m = 0.308$, $h = 0.678$, $\Omega_k = 0$ (Planck Collaboration et al. 2015).

2 IMAGING DATA OF HSC J1152+0047

The lens system, HSC J1152+0047, was recently discovered serendipitously during the visual inspection of data from the HSC Wide (internal data release $\sim 80 \text{ sq. deg.}$, S15A). HSC J1152+0047 consists of the main lens galaxy (G) with four lensed images (A, B, C and D) in a cross configuration (see Fig. 1). A second galaxy (G1) located very close to image C, is probably a satellite of the main lens galaxy G and is likely to perturb the lens potential.

We measured the relative astrometry and photometry of the

¹ According to the Master Lens Database (<http://admin.masterlens.org/index.php>), from a collection of over 115 lensed quasars, about 30 systems are known to be quads.

lens galaxies and the lensed images from the HSC imaging using GALFIT (Peng et al. 2002). In Fig. 2, we show all of the HSC bands and the model-subtracted residual images for each band, respectively. The seeing in the HSC- g, r, i, z and Y images is found to be $0''.55, 0''.46, 0''.45, 0''.60$, and $0''.61$, respectively, as per hscPipe. All of the four lensed images are fit with a point spread function (PSF) model in all bands except in the i -band, where a Sersic profile is better fit to images A and B. The lens galaxy G is fit with a double Sersic model and the companion galaxy G1 is fit with a PSF model. For lens galaxy G, we used the z -band best-fit model as prior when fitting the double Sersic model in other bands. The relative positions from z -band and photometry in all bands along with errors from GALFIT are given in Table 1. We note that the colors ($g - r$ and $r - i$) of the lensed images (see Table 1) are consistent with the colors of a quasar at $z \sim 4$ (Richards et al. 2001).

The flux ratios of images B, C, D with respect to image A are shown in Fig. 3 for all of the HSC *grizY*-bands. The flux ratios appear nearly uniform across all bands with no strong evidence for differential reddening. The flux of image C, however, is likely contaminated by the emission from satellite galaxy (G1) in the reddest (Y) band where G1 becomes more prominent. In the bluer bands, the fluxes of images C and D are comparable as expected for this image configuration from lensing. Although the presence of G1 could affect the magnification of image C, we do not detect any significant difference between relative fluxes of C and D.

We find that our system is also detected in the near-infrared (NIR) imaging taken by the VISTA Kilo-degree Infrared Galaxy survey (VIKING; Edge et al. 2013). The $JHKs$ imaging obtained from the VISTA Science Archive (VSA)² is shown in Fig. 4. The brighter pair of lensed images shows hints of presence in the J and H imaging, where as they are well detected in the Ks -band.

We fit a PSF model to the brighter pair of images and a Sersic model to the galaxy G with GALFIT. We use the 2MASS K -band magnitude of a nearby star for the flux calibration of our VIKING Ks -band photometry. The images A, B and galaxy G have Ks -band magnitudes of $19.31 \pm 0.10, 20.28 \pm 0.27$ and 15.23 ± 0.14 Vega mag, respectively.

We also checked if the lensed source is detected in the Wide-field Infrared Survey Explorer (WISE) imaging (Wright et al. 2010). While W1- and W2-bands show emission at the center of HSC J1152+0047, we cannot confirm the presence of the lensed source due to source confusion owing to the low resolution ($6''$). The source catalog from WISE reports two detections. One of the sources coincides with the lens galaxy G whereas the second source does not coincide with any of the lensed images or galaxy G1 (see Fig. 4). The lens galaxy G has $W1 = 15.18 \pm 0.04$ and $W2 = 15.04 \pm 0.08$ Vega mag, respectively. In bands W3 and W4, there is no detection of any emission either from the lens or the lensed source thus, providing a strong upper limit on source flux. The sensitivities with a signal-to-noise ratio (SNR) of 5 for W3 and W4 bands are 11.5 and 7.87 Vega mag, respectively.

3 SPECTROSCOPIC OBSERVATION OF HSC J1152+0047

We obtained spectra of HSC J1152+0047 on 2016 March 11 with Gemini North Telescope through the Fast Turnaround program (Mason et al. 2014) with seeing around $0''.6$ - $0''.7$. We used GMOS

Table 1. Relative astrometry and photometry of HSC J1152+0047 using GALFIT.

Name	Δx err	Δy err	g err	r err	i err	z err	Y err
A	0.0	0.0	24.23	23.10	22.82	22.82	22.80
	—	—	0.06	0.02	0.02	0.02	0.04
B	-3.85	-1.34	24.32	23.12	22.87	22.79	22.86
	0.01	0.01	0.06	0.02	0.02	0.02	0.04
C	-1.52	-1.87	24.76	23.71	23.49	23.29	23.50
	0.02	0.02	0.10	0.05	0.03	0.03	0.15
D	-2.45	0.70	24.71	23.61	23.41	23.27	23.19
	0.01	0.01	0.10	0.05	0.03	0.03	0.07
G	-1.96	-0.57	21.85	20.31	19.52	19.15	19.05
	0.01	0.01	0.12	0.05	0.05	0.02	0.03
G	-2.04	-0.47	21.63	20.27	19.43	19.18	19.06
	0.01	0.02	0.22	0.03	0.12	0.03	0.03
G1	-1.25	-2.36	25.87	24.43	23.62	23.22	23.01
	0.01	0.02	0.24	0.07	0.03	0.04	0.11

The position of image A is RA,Dec=(178.21722, 0.79271) deg. The relative astrometry is from the z -band in units of arcsec. The positive directions of Δx and Δy are North and West, respectively. For every object, the second row shows the errors from GALFIT. Except the i -band for images A and B where a Sersic model is chosen, all of the lensed images are fit with a PSF model. The magnitudes are corrected for Galactic extinction.

in the long-slit mode with R400-G5305 grating and GG455 blocking filter. The width of the slit was set to $1''.0$. This provides a spectral resolution $R=1918$ and wavelength coverage from 4000 to 8000 Å. Two perpendicular slit configurations were used to acquire spectra of all 4 lensed images, as well as the lens galaxy G. The brighter pair was observed for 15 min and the fainter pair was observed for 45 min. The companion galaxy G1 is aligned with the fainter pair and fell on the second slit but was too faint to be detected.

We carried out the data reduction using IRAF with the dedicated GMOS package (v1.13). The spectra were bias subtracted, flat fielded and sky subtracted. We used CuAr lamp to calibrate the wavelength. Because the lensed image spectra are very faint and close to the spectra of the lens galaxy ($<2''$ for the brighter pair, and $<1''$ for the fainter pair), we manually select the aperture size and spectra position to extract the lensed image spectra. This is done using the ‘gsextract’ routine in an interactive mode. For the fainter pair, the spectra are dominated by the lens galaxy light. To avoid contamination from the lens for the fainter pair of images, we scaled the red part (> 7000 Å) of the lens spectrum to match the spectrum of the fainter images assuming that most of the redder part is dominated by the emission from the lens. We then subtracted this normalized lens galaxy spectrum from the spectra of the fainter images. We calibrate the flux based on spectroscopic standard star. We estimate flux errors using the variance at each pixel, which is calculated from the raw image, and taking into account the effects of each reduction step using error propagation, till extracting the one-dimensional spectra.

The spectra of the lens galaxy and the four lensed images are shown in Fig. 5. The spectra of each of the lensed images in the figure are smoothed with a Gaussian filter of 2.7 Å and vertical offsets are added for illustrative purpose. The redshift of the lens galaxy is found to be $z_1 = 0.466 \pm 0.001$ through the identifica-

² <http://horus.roe.ac.uk/vsa/dboverview.html>

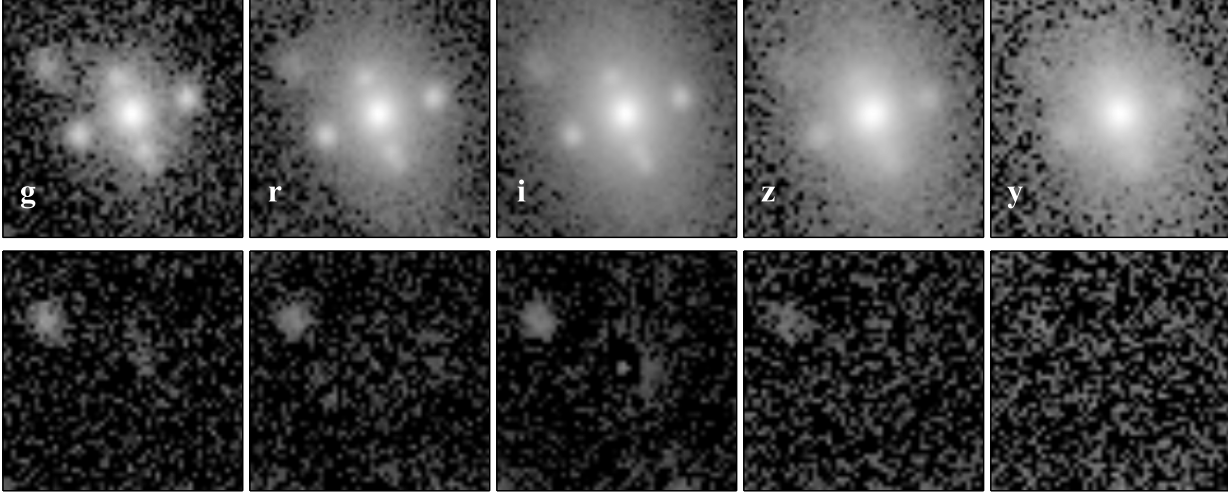


Figure 2. GALFIT modeling results in HSC *grizY*-bands. Top panels show the HSC images whereas the bottom panels show GALFIT model subtracted residual images in the respective bands. Images are $9''$ on the side.

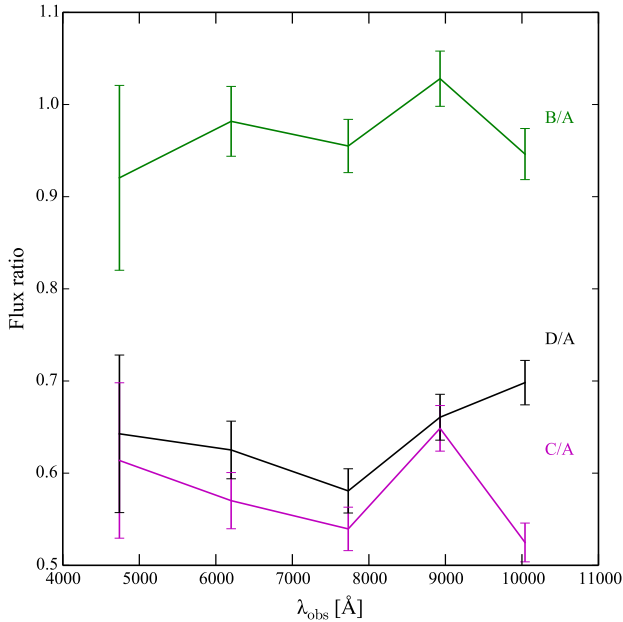


Figure 3. Flux ratios of the lensed images as a function of wavelengths from the HSC *grizY*-band data (see also Table 1).

tion of CaII H and K absorption lines near the 4000 \AA break as expected for a typical early-type galaxy. As mentioned earlier, we do not have a spectrum of G1 but our photometric redshift estimate ($z_{\text{IG1}} = 0.46 \pm 0.15$) suggests that G1 is a gravitationally bound satellite of galaxy G. The similarity in the spectra of the four images confirms the strong lensing nature of this system. The redshift of the lensed source is found to be $z_s = 3.76 \pm 0.01$ based on the identification of the Ly- α emission line. Also, the stacked spectrum shows other high ionization state emission lines e.g., NV and C IV which are rather weak but their presence is consistent with the interpretation of the stronger emission line as Ly- α (see Fig. 5).

4 LENS MASS MODELING

We used the lens modeling software GLAFIC (Oguri 2010) for lens mass modeling. We started with *i*-band HSC image where information from each pixel offer data constraints for the mass models.

The lens galaxies are each modeled with an isothermal density profile. Galaxy G is allowed to have ellipticity whereas galaxy G1 is assumed to have spherically symmetric mass distribution since G1 is less massive and the contribution from the quadrupole moment of its mass distribution is not expected to be significant. While we allowed for external shear to be present earlier in our models, we found that this was highly degenerate with the ellipticity of G and did not improve the fit significantly. Hence, we removed it for simplicity. Thus, our final lens mass model consists of an isothermal ellipsoid (SIE) for G and an isothermal sphere (SIS) for G1.

We tested different assumptions when modeling the light profile of the lensed source. Our list of models comprised i) single PSF ii) single Sersic and iii) PSF+Sersic. We found that a single PSF model left significant residuals in the *i*-band image, as expected and a PSF+Sersic model was not an improvement over the single Sersic model. Therefore, our final best model for the lensed source is a single Sersic component.

We run Monte Carlo Markov Chain (MCMC) using EMCEE (Foreman-Mackey et al. 2013). The model fitting includes pixels within a $7''$ box centered on the lens (see left panel of Fig. 6). The medians of the posterior distributions of our model parameters are given in Table 2. We only report the source magnitude and effective radius from our model in Table 2 since other source parameters such as the ellipticity and position angle (PA) are not well-constrained. Also, since the Sersic index n was not well-constrained we fixed it to $n = 4$ that corresponds to the de Vaucouleurs' profile.

In Fig. 6, we show the model image (middle panel) and the residual image (right panel) after subtracting the model from the data. We also show critical curves (white contours) and caustics (magenta contours) marking the regions of infinite magnification in the middle panel. We highlight the peak positions of the model-predicted lensed images (circles) and the true source position (triangle).

Finally, we also constructed mass models by fitting to just the

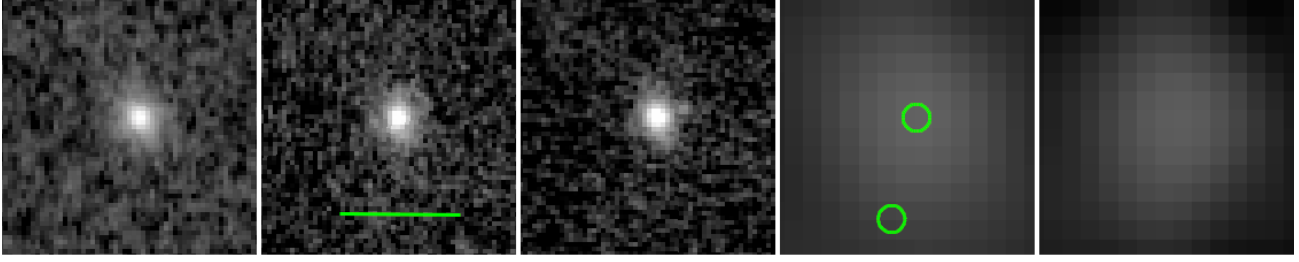


Figure 4. From left to right, NIR VIKING imaging in Filters (limiting AB magnitudes) $J(22.1)$, $H(21.5)$, and $Ks(21.2)$ followed by WISE imaging in bands W1 and W2. The brighter pair of lensed images are close to the detection limits of VIKING J and H imaging whereas they are detected in the Ks -band. W1 and W2 imaging show emission from the lens galaxy alone (see Section 2). The two green circles mark the location of sources detected from the WISE catalogs. North is up and East is left. The bar shows a scale of $9''$.

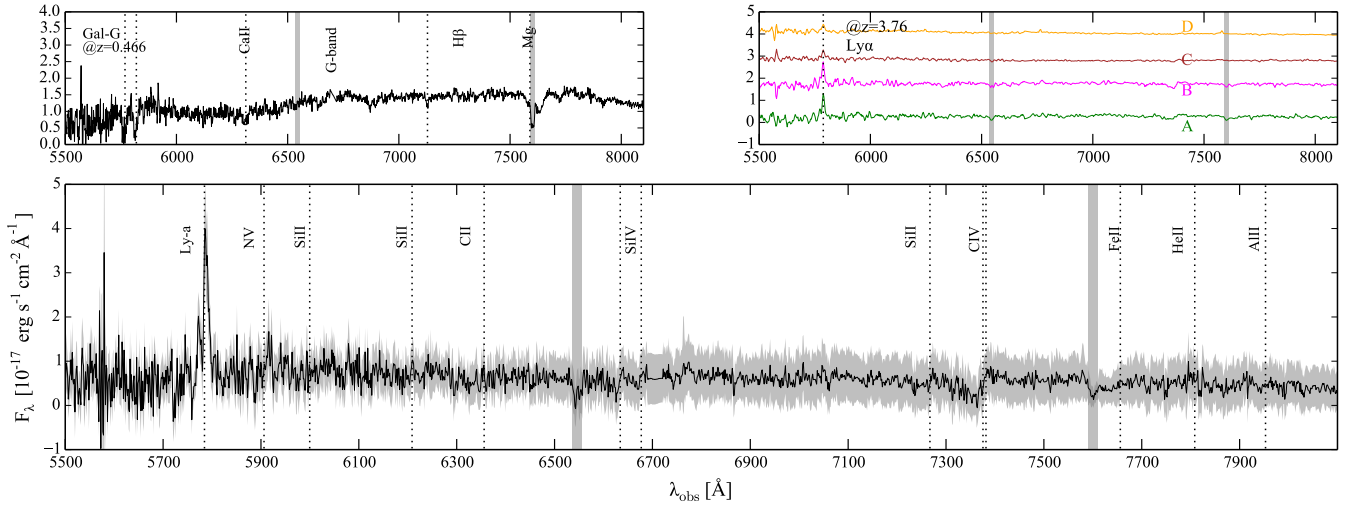


Figure 5. *Upper left:* The spectrum of the lensing galaxy from our Gemini GMOS spectroscopic follow-up observation. The lens redshift is $z_1 = 0.466$. *Upper right:* Individual binned spectra of the lensed images A–D from the Gemini GMOS spectroscopy. All the images have the Ly- α emission line redshifted to $z_s = 3.76$. *Lower:* The stacked spectrum of the lensed source with commonly found emission and absorption lines labelled. The error on the spectrum is shown with the shaded region (grey). The two vertical bars (grey) shown in all panels indicate absorption features probably due to telluric contamination.

Table 2. Mass modeling results from fitting a lensed extended source to i -band image.

Parameters	Values (units)
Velocity dispersion (G)	$280 \pm 10 \text{ km s}^{-1}$
Ellipticity (G)	0.54 ± 0.02
PA of Ellipticity (G)	$19.1 \pm 0.5 \text{ deg}$
Velocity dispersion (G1)	$100 \pm 30 \text{ km s}^{-1}$
True Source magnitude	23.9 ± 0.1
True Source Effective radius	$0.028 \pm 0.005 \text{ arcsec}$

peak positions and relative fluxes of the lensed images which were measured with GALFIT. We tested similar lens models as before except that the source is assumed to be a point source since the data constraints are limited. From this analysis, we determined a magnification factor of $\mu = 2.5 - 3$ for images A and B. We choose $\mu = 2.5^3$ for the analysis presented in Section 5.

³ We note that choosing $\mu = 3$ does not qualitatively change our conclusions about the source properties.

Table 3. Properties of Ly- α for the brighter pair of lensed images.

Name	EW \AA	FWHM km s^{-1}	$L \times 10^{42}$ ergs s^{-1}
A	$16 \pm 1 (30)$	$540 \pm 40 (920)$	3.2 (6.3)
B	$15 \pm 1 (26)$	$640 \pm 50 (890)$	3.2 (6.3)

The values are given for the narrow component of Ly- α and the values within parentheses are given for the broader component. The EW is given in the rest-frame. The luminosities are dereddened by taking into account the magnification factor.

5 RESULTS

In this section, we determine the properties of the lensed source based on the modeling of the imaging and spectroscopic data. First, we analyze the single most prominent emission line found in the spectra of the lensed images. Next, we determine the true source magnitude and size to decide whether the source is dominated by an AGN or not.

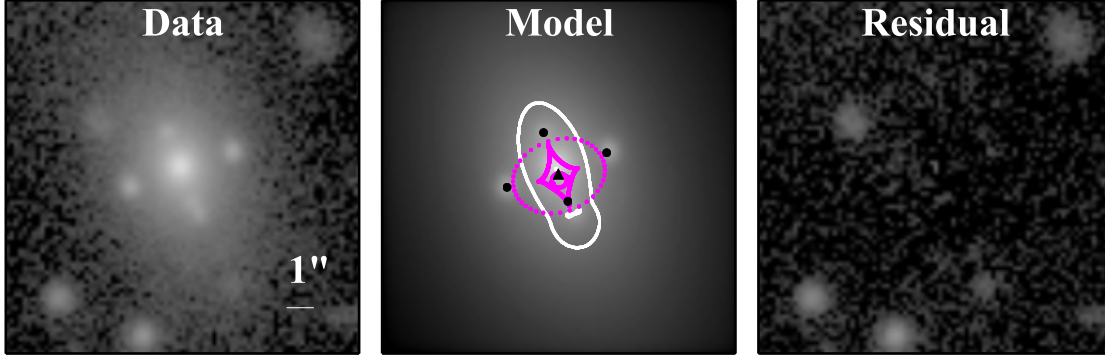


Figure 6. HSC *i*-band image (left), lens mass model where the background source is assumed to have a Sersic profile (middle) and the residual image (right). The middle panel also shows the positions of the lensed images (circles) and the source (triangle). The magenta contours show the caustics in the source plane and white contours mark the corresponding critical curves in the image plane indicating regions of extremely high magnification.

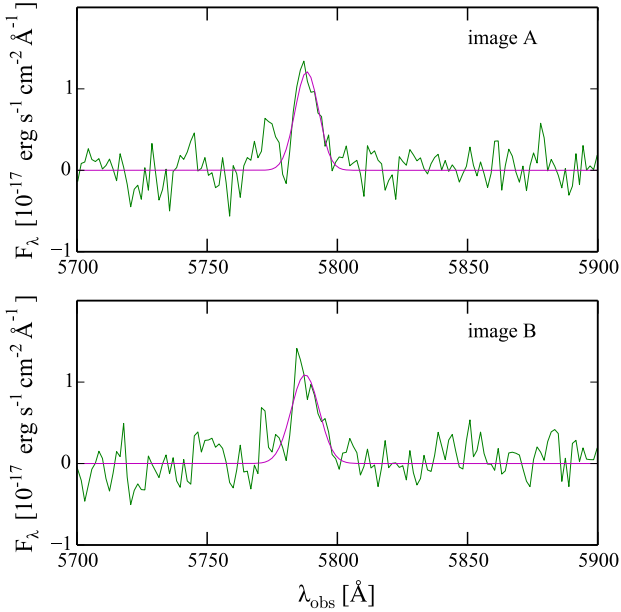


Figure 7. One-dimensional Gaussian fit to Ly- α of image A (upper) and image B (lower).

5.1 Ly- α emission

We fit a Gaussian to the one-dimensional spectrum around the Ly- α emission in images A and B (see Fig. 7). We obtain a line width of $\sigma = 4.6 \pm 0.3 \text{ \AA}$ and $5.4 \pm 0.4 \text{ \AA}$ at 5788 \AA , respectively. Given the spectral resolution ($R = 1918$), the instrumental broadening corresponds to 156 km s^{-1} . Thus, the Full-Width at Half-Maximum (FWHM) of Ly- α emission from images A and B, after accounting for the instrumental broadening, is $540 \pm 40 \text{ km s}^{-1}$ and $640 \pm 50 \text{ km s}^{-1}$, respectively. There is a second peak blueward of the Ly- α line, which suggests that the underlying Ly- α is much broader, with different parts of the emission line modified by absorption or scattering from surrounding neutral hydrogen. This absorption feature is more obvious for image A than image B. The FWHMs of the broader Ly- α line (including the second peak to the left) of images A and B are ~ 920 and $\sim 890 \text{ km s}^{-1}$, respectively.

This is also consistent with the FWHM estimate measured from the stacked (unbinned) spectra of the four images.

The flux of the Ly- α line from a flux-calibrated spectrum of image A is $1.4 \times 10^{-16} \text{ ergs s}^{-1} \text{ cm}^{-2}$ which gives a luminosity of $10^{42.5} \text{ ergs s}^{-1}$ after taking into account the magnification factor μ of 2.5. The equivalent width (EW) of Ly- α line is $75 \pm 5 \text{ \AA}$ in the observed frame and $16 \pm 1 \text{ \AA}$ in the rest frame for image A. The errors represent 68% confidence levels on the posterior distribution of the parameters sampled with MCMC. We present the measurements for both the narrow and the broad components of Ly- α in Table 3.

5.2 Source Magnitude

GALFIT model fitting to image A in the *i*-band suggested $i = 22.82$. Using the magnification factor of $\mu = 2.5$, we obtain a delensed source magnitude of $i = 23.84$. At $z_s = 3.76$, this corresponds to an absolute magnitude $M_{1500} = -22.1$ after applying a K-correction for the quasar continuum $K_{\text{corr}} = -2.5 (1 + \alpha) \log (1 + z_s) - 2.5 \alpha \log (1500 \text{ \AA} / \lambda_{\text{eff}})$ following the prescription of Glikman et al. (2010) where $\alpha = -0.5$ (Richards et al. 2006).

Alternatively, we can determine the true source magnitude from the results of our lens mass modeling by fitting an extended source to the *i*-band image. The best-fit source magnitude thus obtained, is $i = 23.9 \pm 0.1$ which corresponds to $M_{\text{UV}} = -22.0 \pm 0.1$.

5.3 Source size

We followed the same two approaches as before to estimate the true source size. GALFIT model fitting suggested a size of $r_{\text{eff},l} = 0''.12$ where subscript *l* suggests lensed. The lensing magnification factor ($\mu = 2.5$) is used to scale down the area of the lensed source to get the true source size. We assume the source is circular (i.e. $\text{area} = \pi r_{\text{eff},t}^2$ where subscript *t* implies true) and that the lensing magnification is the same in all directions. Thus, the true source size is estimated to be $r_{\text{eff},t} = \sqrt{r_{\text{eff},l}^2 / \mu} = 0''.069$. Given the physical scale at $z_s = 3.76$ of $7.33 \text{ kpc arcsec}^{-1}$, the source size is $\sim 0.56 \text{ kpc}$ in physical units.

The best-fit source size $r_{\text{eff},t}$ from lens mass modeling is found to be even smaller, $\sim 0''.028 \pm 0''.005$, suggesting a physical

source size of 0.20 ± 0.04 kpc. We trust our latter estimate more because the former estimate has a larger systematic error owing to the strong assumptions adopted in our calculation.

6 DISCUSSION

In this section, we make a comparison of properties of high redshift population of galaxies and AGNs with the lensed source of HSC J1152+0047 to better understand its nature. We also discuss possible sources of chromatic (i.e. wavelength dependent) variations seen in the flux ratio of the brighter pair of lensed images.

6.1 Comparison with Ly- α emitter (LAEs)

LAEs are star-forming galaxies with faint ultra-violet (UV) continuum and a prominent Ly- α emission line (e.g. Malhotra & Rhoads 2002; Ouchi et al. 2008; Shibuya et al. 2012).

LAEs are known to have large $EW_{Ly-\alpha}$ and small velocity widths $\Delta v_{Ly-\alpha}$ (e.g., Ouchi et al. 2008; Hashimoto et al. 2013). For example, rest-frame $EW_{Ly-\alpha}$ for a sample of LAEs at $z \sim 3.7$ is $> 44 \text{ \AA}$ (Ouchi et al. 2008) much larger than that of our lensed source but their sample is limited by the selection effects of their narrow-band data. Usually LAEs are defined to be high-redshift galaxies with rest-frame $EW_{Ly-\alpha} \geq 20 \text{ \AA}$ (e.g., Ouchi et al. 2003). Thus, our source is probably at the border of being an LAE based on the EW criteria. Ouchi et al. (2010) measured velocity widths of Ly- α for a large sample of over 200 Ly- α emitter (LAEs) at high redshifts. They find average velocity widths of 260 km s^{-1} without significant difference between $z = 5.7 - 6.6$. Assuming that this holds true at $z \sim 4$, the FWHM of Ly- α for the source in HSC J1152+0047 is much broader to be an LAE type of galaxy.

The Ly- α luminosity of our source is within the range of LAEs of $10^{41-44} \text{ ergs s}^{-1}$ although on the fainter end. For example, if we compare the Ly- α luminosity function of LAEs (e.g. Ouchi et al. 2008), the characteristic luminosity $L_{Ly-\alpha}^* = 10.2 \times 10^{42} \text{ ergs s}^{-1}$ at $z = 3.7$. Our source with $L_{Ly-\alpha} = 3.16 \times 10^{42} \text{ ergs s}^{-1}$ is $0.3L^*$ of the LAE population. Furthermore, the sizes of LAEs are found to be of the order of $\sim 1 \text{ kpc}$ (e.g., Pirzkal et al. 2007; Overzier et al. 2008) at $z \sim 4$. Nevertheless, our source is much more compact than most of the LAEs.

6.2 Comparison with Lyman Break Galaxies (LBGs)

The characteristic of LBGs is a sharp drop in the flux bluewards of the Ly- α . We do not see any strong evidence of such a sharp cut-off in either the spectrum (see Fig. 7) or the imaging although its colors may not be inconsistent with an LBG (e.g., Bouwens et al. 2014). On the other hand, the spectrum lacks strong metal-line emission and shows some absorption features (e.g. bluewards of C IV, possibly S IV). Hence, we compare our source with other LBGs.

Shibuya et al. (2015) derived the size-magnitude (M_{UV}) relation for SFGs and LBGs at $z \sim 4$ (as shown in Figure 9 of their paper). Our source is an outlier for the $z \sim 4$ population and does not show expected size and magnitude properties for either SFGs or LBGs at that redshift. In fact, it is extremely compact and at the brighter end of the rest of the population suggesting that the source probably has an AGN with low-to-moderate luminosity.

We note that morphologies of most of the known lensed LBGs appear well-extended in the form of arcs although with high surface brightness compared to regular SFGs (e.g., Seitz et al. 1998; Allam et al. 2007; Diehl et al. 2009; Koester et al. 2010). In fact, the size

of our source is too compact and is comparable to lensed LBGs at $z \sim 6 - 8$ (Bradley et al. 2008; Kawamata et al. 2015).

6.3 Comparison with (lensed or red) Quasars

In addition to Ly- α , AGNs typically show high ionization-state emission lines such as NV $\lambda 1240$, C IV $\lambda 1549$ and He II $\lambda 1640$ produced in the Broad line regions (BLR) or narrow line regions (NLR). While the spectra of each of the lensed images do not show any other prominent emission lines, the stacked spectrum (see Fig. 5) reveals presence of NV and C IV with absorption on the bluer side. This is similar to the doubly lensed quasar of SDSS J094604.90+183541.8 (McGreer et al. 2010) at $z = 4.8$ which shows weak C IV with absorption of the blue wing.

Even though uncommon, we note that a few AGNs with Ly- α emission only have been reported in the literature. For example, Hall et al. (2004) reported a very unusual radio-loud AGN showing Ly- α emission line alone in its spectrum without the presence of any strong metal emission lines. Among the high- z lensed quasars, CY 2201-3201 is a doubly lensed quasar at $z = 3.9$ and also shows only Ly- α in its spectrum (Castander et al. 2006). It also has r and i magnitudes comparable to HSC J1152+0047. However, CY 2201-3201 is detected in X-rays albeit with moderately deep (~ 50 kilosecond) *Chandra* imaging $L_X = 1.49 \times 10^{44} \text{ ergs s}^{-1}$ in the soft band (0.52.0 keV). HSC J1152+0047, on the other hand, is neither detected in archival X-ray (RASS) nor in archival radio (NVSS and FIRST) data⁴. However given that this might be a low luminosity AGN, we would need deeper X-ray imaging to verify the presence of an AGN similar to that required to detect CY 2201-3201.

Our lensed source satisfies the optical-color criterion of Fynbo et al. (2013) used for selecting red quasars and has similar SED to a few broadline quasars at around $z = 3.6 - 3.7$ from their sample except that the emission lines are narrower and weaker in our source and it is ~ 3.5 magnitudes fainter than the high- z quasars of Fynbo et al. (2013).

6.4 Chromatic variations in the flux ratios

6.4.1 Intrinsic variability due to AGN

AGNs are known to show intrinsic variability over months to years whereas galaxies do not have any mechanism to produce variability on such time scales, except when they host luminous transients such as supernovae. We find that the flux ratio of the brighter image pair ($B/A \sim 0.41 \pm 0.11$) in K -band is discrepant with the ratio of 0.95 ± 0.02 seen in the HSC data. From the geometrical symmetry of the lensed images in an Einstein cross and from our mass models, the relative time delay in the arrival of light rays between the brighter pair of the lensed images is a few days. The difference of 1 magnitude within a period of a few days is too rapid to be caused by intrinsic flux variation in the AGN.

6.4.2 Finite source size

The lensed images appear point-like in both optical and NIR whenever detected except that the brighter pair of images indicate extendedness in HSC i -band (see Section 2). Thus, we consider the

⁴ RASS stands for ROSAT All Sky Survey. NVSS stands for NRAO VLA All Sky Survey. FIRST stands for Faint Images of the Radio Sky at Twenty-Centimeters.

scenario where we detect the host galaxy with a finite size and we are seeing different regions of the source in the optical and NIR which might explain different flux ratios. However, for an Einstein-Cross, the source is located very close to the lens center, inside the diamond caustics (see Fig. 6) and small changes in the source position are not expected to produce significant changes in the image magnification for images A and B. Nevertheless, we calculated by how much the magnification would vary if the source emission arises from spatially distinct regions offset by a small amount. We compared the angular separations of images A and B with respect to the lens galaxy G between the HSC z and VIKING K s-bands and found an offset of $0''.08$. The change in the magnification, if images A and B are offset at a scale of $0''.1$, is $< 10\%$ (i.e. a magnitude difference of < 0.1). Thus, the variation in flux ratios between optical and K s-bands cannot be explained by emission arising from different regions of the source.

6.4.3 Microlensing and Millilensing

Microlensing is the lensing effect produced by very low mass compact components, for example, from stars, globular clusters or black holes in the plane of a lens galaxy. Microlensing could produce chromatic variations in flux ratios. This effect is sensitive to the scale of the source size. The size of region emitting rest-frame optical (observed frame NIR) in the source plane is much larger than that of the region emitting rest-frame UV (observed frame optical). Thus, the K s-band fluxes are expected to be less affected by microlensing. However, HSC J1152+0047 shows a discrepancy in the K s-band flux ratio instead of the optical.

Also, the VIKING Z -band (not shown here) suggests a flux ratio, $B/A \sim 1$ consistent with HSC data. The VIKING K s-band data were taken 1 yr after VIKING Z -band data and HSC data were taken 4 yrs after K s-band data. Ignoring the fact that we are comparing data in different bands here, these timescales even though short are still feasible for microlensing to appear, based on the caustic crossing time estimated by following Treyer & Wambsgans (2004).

Microlensing can also be deduced by comparing the continuum and emission line flux ratios (e.g. Sluse et al. 2007). The ratio of the flux calibrated optical spectra of images A and B is nearly one, both for the continuum and the Ly- α emission line disfavoring the microlensing scenario. However, high resolution and deeper spectroscopy is needed to rule out microlensing with certainty. Therefore, microlensing does not seem to be the obvious explanation of the discrepancy in the flux ratios between the optical and NIR but cannot be ruled out completely without additional data.

Millilensing is the lensing effect produced at an angular scale of milli-arcseconds due to dark subhalos or luminous satellite galaxies of low mass ($\sim 10^{6-10} M_{\odot}$). Millilensing effect can cause deviation from the expected flux ratios of the brighter pair but this effect is achromatic and cannot be the cause of variable flux ratios.

6.4.4 Differential Extinction

Extinction from the presence of dust in the lens galaxy could affect the flux ratios as a function of the wavelength. Firstly, the lens galaxy is an early-type galaxy which does not have significant dust to cause severe extinction of the lensed images (e.g. Falco et al. 1999; Elíasdóttir et al. 2006). Given that the system is fairly symmetrical in the near North-South direction and that images A and

B are almost equidistant on the either side of the lens galaxy, the amount of dust is not expected to be significantly different to cause such a high level of differential extinction in the lensed images A and B and in the K s-band alone. Also, extinction affects strongly at shorter wavelengths but the flux ratio, B/A does not show any sign of extinction in the HSC data. Thus, extinction is unlikely to be the source of variability seen in HSC J1152+0047.

7 CONCLUSION

We have discovered a quadruply imaged source from the HSC survey at $z_s = 3.76$ lensed by an early-type galaxy at $z_l = 0.466$. The source colors and SED are similar to other red or high- z quasars although the color may also be consistent with that of an LBG. If the source indeed has an AGN, then this represents the highest redshift quadruply lensed AGN. The rest-frame UV spectrum shows weak metal emission lines (NV and blue-wing absorbed C IV) found in the NLR/BLR around AGNs. The Ly- α emission line is narrow but broader than velocity widths typically found in LAEs and LBGs and its luminosity is consistent with a faint AGN. Faint AGNs are useful to study quasar fueling lifetime, feedback and faint end slope of the luminosity function (e.g., Hopkins et al. 2006; Glikman et al. 2010; Fiore et al. 2012; Ikeda et al. 2012; Matsuoka et al. 2016).

While the lensed source is faint, the delensed absolute UV magnitude is at the brighter end of SFG and LBG population. Moreover, the source appears point-like in most bands, the HSC i -band suggests extendedness for the brighter pair of lensed images in the tangential direction which could suggest that we are detecting emission from the underlying AGN host. The effective radius of the source from our lens modeling is very small. In fact, it is the most compact source compared to other SFG and LBGs at $z \sim 4$. We do not see any sign of variability in the four lensed images from the HSC data but the VIKING K s-band data show highly discrepant flux ratio for the brighter pair. The origin of the chromatic variation is not understood since none of the known phenomena such as intrinsic variability, microlensing and differential extinction can fully explain the measured optical and NIR flux ratios. We do not rule out microlensing due to lack of sufficient data. We need high resolution and high SNR spectrum to better quantify the relative strengths of the emission lines, to see signatures of microlensing.

In general, following investigations will help shed light on the true nature of the source. Deep X-ray imaging will allow us to decide whether the source of Ly- α is due to an AGN (e.g. Malhotra et al. 2003). IR spectroscopy will facilitate detection of Mg-II $\lambda 2800$, if any, confirming the presence of the AGN and providing an estimate of the black hole mass. High resolution (space or adaptive optics from ground) imaging will give a better understanding of the morphology of the source, for instance, whether we are seeing the host and an AGN or just a compact galaxy. We will also be able to put more stringent constraints on the physical size of this highly compact source. This discovery from the HSC data of probably the first low-luminosity lensed AGN shows promise for many interesting discoveries to occur in the near future.

ACKNOWLEDGMENTS

AM is supported by World Premier International Research Center Initiative (WPI Initiative), MEXT, Japan. MO is supported by JSPS KAKENHI Grant Number 26800093 and 15H05892. S.H.S. is supported by the Max Planck Society through the Max Planck Re-

search Group. S.H.S. and J.H.H.C. acknowledge support from the Ministry of Science and Technology in Taiwan via grant MOST-103-2112-M-001-003-MY3. A.S. acknowledges support by JSPS KAKENHI Grant Number 26800098. AM would like to thank T. Anguita, L. Hao, Y. Harikane, S. Huang, D. Sluse and M. Strauss for useful discussion. The Hyper Suprime-Cam (HSC) collaboration includes the astronomical communities of Japan and Taiwan, and Princeton University. The HSC instrumentation and software were developed by the National Astronomical Observatory of Japan (NAOJ), the Kavli Institute for the Physics and Mathematics of the Universe (Kavli IPMU), the University of Tokyo, the High Energy Accelerator Research Organization (KEK), the Academia Sinica Institute for Astronomy and Astrophysics in Taiwan (ASIAA), and Princeton University. Funding was contributed by the FIRST program from Japanese Cabinet Office, the Ministry of Education, Culture, Sports, Science and Technology (MEXT), the Japan Society for the Promotion of Science (JSPS), Japan Science and Technology Agency (JST), the Toray Science Foundation, NAOJ, Kavli IPMU, KEK, ASIAA, and Princeton University. This paper makes use of software developed for the Large Synoptic Survey Telescope. We thank the LSST Project for making their code available as free software at <http://dm.lsstcorp.org>. The Pan-STARRS1 Surveys (PS1) have been made possible through contributions of the Institute for Astronomy, the University of Hawaii, the Pan-STARRS Project Office, the Max-Planck Society and its participating institutes, the Max Planck Institute for Astronomy, Heidelberg and the Max Planck Institute for Extraterrestrial Physics, Garching, The Johns Hopkins University, Durham University, the University of Edinburgh, Queen's University Belfast, the Harvard-Smithsonian Center for Astrophysics, the Las Cumbres Observatory Global Telescope Network Incorporated, the National Central University of Taiwan, the Space Telescope Science Institute, the National Aeronautics and Space Administration under Grant No. NNX08AR22G issued through the Planetary Science Division of the NASA Science Mission Directorate, the National Science Foundation under Grant No. AST-1238877, the University of Maryland, and Eotvos Lorand University (ELTE). Based on observations obtained at the Gemini Observatory, which is operated by the Association of Universities for Research in Astronomy, Inc., under a cooperative agreement with the NSF on behalf of the Gemini partnership: the National Science Foundation (United States), the National Research Council (Canada), CONICYT (Chile), Ministerio de Ciencia, Tecnología e Innovación Productiva (Argentina), and Ministério da Ciência, Tecnologia e Inovação (Brazil). The authors wish to recognize and acknowledge the very significant cultural role and reverence that the summit of Mauna Kea has always had within the indigenous Hawaiian community. We are most fortunate to have the opportunity to conduct observations from this mountain. This research has made use of the NASA/IPAC Infrared Science Archive, which is operated by the Jet Propulsion Laboratory, California Institute of Technology, under contract with the National Aeronautics and Space Administration.

REFERENCES

- Allam, S. S., Tucker, D. L., Lin, H., Diehl, H. T., Annis, J., Buckley-Geer, E. J., & Frieman, J. A. 2007, *ApJ*, 662, L51
- Atek, H., et al. 2015, *ApJ*, 814, 69
- Axelrod, T., Kantor, J., Lupton, R. H., & Pierfederici, F. 2010, in *Proc. SPIE*, Vol. 7740, *Software and Cyberinfrastructure for Astronomy*, 774015
- Bonvin, V., et al. 2016, *ArXiv e-prints*
- Bouwens, R. J., et al. 2014, *ApJ*, 793, 115
- Bradley, L. D., et al. 2008, *ApJ*, 678, 647
- . 2014, *ApJ*, 792, 76
- Browne, I. W. A., et al. 2003, *MNRAS*, 341, 13
- Castander, F. J., Treister, E., Maza, J., & Gawiser, E. 2006, *ApJ*, 652, 955
- Dalal, N., & Kochanek, C. S. 2002, *ApJ*, 572, 25
- Diehl, H. T., et al. 2009, *ApJ*, 707, 686
- Edge, A., Sutherland, W., Kuijken, K., Driver, S., McMahon, R., Eales, S., & Emerson, J. P. 2013, *The Messenger*, 154, 32
- Egami, E., et al. 2005, *ApJ*, 618, L5
- Elíasdóttir, Á., Hjorth, J., Toft, S., Burud, I., & Paraficz, D. 2006, *ApJS*, 166, 443
- Falco, E. E., Gorenstein, M. V., & Shapiro, I. I. 1985, *ApJ*, 289, L1
- Falco, E. E., et al. 1999, *ApJ*, 523, 617
- Fiore, F., et al. 2012, *A&A*, 537, A16
- Foreman-Mackey, D., Hogg, D. W., Lang, D., & Goodman, J. 2013, *PASP*, 125, 306
- Fynbo, J. P. U., Krogager, J.-K., Venemans, B., Noterdaeme, P., Vestergaard, M., Møller, P., Ledoux, C., & Geier, S. 2013, *ApJS*, 204, 6
- Glikman, E., Bogosavljević, M., Djorgovski, S. G., Stern, D., Dey, A., Jannuzi, B. T., & Mahabal, A. 2010, *ApJ*, 710, 1498
- Hall, P. B., et al. 2004, *AJ*, 127, 3146
- Hashimoto, T., Ouchi, M., Shimasaku, K., Ono, Y., Nakajima, K., Rauch, M., Lee, J., & Okamura, S. 2013, *ApJ*, 765, 70
- Hopkins, P. F., Hernquist, L., Cox, T. J., Robertson, B., Di Matteo, T., & Springel, V. 2006, *ApJ*, 639, 700
- Huang, K.-H., et al. 2016, *ApJ*, 817, 11
- Ikeda, H., et al. 2012, *ApJ*, 756, 160
- Inada, N., et al. 2012, *AJ*, 143, 119
- Ivezic, Z., et al. 2008, *ArXiv e-prints*
- Jackson, N., Rampadarath, H., Ofek, E. O., Oguri, M., & Shin, M.-S. 2012, *MNRAS*, 419, 2014
- Jiménez-Vicente, J., Mediavilla, E., Kochanek, C. S., & Muñoz, J. A. 2015, *ApJ*, 799, 149
- Jurić, M., et al. 2015, *ArXiv e-prints*
- Kawamata, R., Ishigaki, M., Shimasaku, K., Oguri, M., & Ouchi, M. 2015, *ApJ*, 804, 103
- Koester, B. P., Gladders, M. D., Hennawi, J. F., Sharon, K., Wuyts, E., Rigby, J. R., Bayliss, M. B., & Dahle, H. 2010, *ApJ*, 723, L73
- Magnier, E. A., et al. 2013, *ApJS*, 205, 20
- Malhotra, S., & Rhoads, J. E. 2002, *ApJ*, 565, L71
- Malhotra, S., Wang, J. X., Rhoads, J. E., Heckman, T. M., & Norman, C. A. 2003, *ApJ*, 585, L25
- Mason, R. E., Côté, S., Kissler-Patig, M., Levenson, N. A., Adamson, A., Emmanuel, C., & Crabtree, D. 2014, in *Proc. SPIE*, Vol. 9149, *Observatory Operations: Strategies, Processes, and Systems V*, 914910
- Matsuoka, Y., et al. 2016, *ArXiv e-prints*
- McGreer, I. D., et al. 2010, *AJ*, 140, 370
- Miyazaki, S., et al. 2012, in *Proc. SPIE*, Vol. 8446, *Ground-based and Airborne Instrumentation for Astronomy IV*, 84460Z
- More, A., et al. 2016, *MNRAS*, 456, 1595
- Morgan, C. W., Kochanek, C. S., Dai, X., Morgan, N. D., & Falco, E. E. 2008, *ApJ*, 689, 755
- Motta, V., Mediavilla, E., Falco, E., & Muñoz, J. A. 2012, *ApJ*, 755, 82
- Myers, S. T., et al. 2003, *MNRAS*, 341, 1

- Nierenberg, A. M., Treu, T., Wright, S. A., Fassnacht, C. D., & Auger, M. W. 2014, *MNRAS*, 442, 2434
- Oguri, M. 2007, *ApJ*, 660, 1
- . 2010, *PASJ*, 62, 1017
- Oguri, M., Rusu, C. E., & Falco, E. E. 2014, *MNRAS*, 439, 2494
- Oguri, M., et al. 2006, *AJ*, 132, 999
- Ouchi, M., et al. 2003, *ApJ*, 582, 60
- . 2008, *ApJS*, 176, 301
- . 2010, *ApJ*, 723, 869
- Overzier, R. A., et al. 2008, *ApJ*, 673, 143
- Peng, C. Y., Ho, L. C., Impey, C. D., & Rix, H.-W. 2002, *AJ*, 124, 266
- Pirzkal, N., Malhotra, S., Rhoads, J. E., & Xu, C. 2007, *ApJ*, 667, 49
- Planck Collaboration et al. 2015, *ArXiv e-prints*
- Rawle, T. D., et al. 2014, *ApJ*, 783, 59
- Refsdal, S. 1964, *MNRAS*, 128, 307
- Richards, G. T., et al. 2001, *AJ*, 121, 2308
- . 2006, *AJ*, 131, 2766
- Riechers, D. A., Carilli, C. L., Walter, F., & Momjian, E. 2010, *ApJ*, 724, L153
- Rusu, C. E., et al. 2016, *MNRAS*, 458, 2
- Schechter, P. L., Pooley, D., Blackburne, J. A., & Wambsganss, J. 2014, *ApJ*, 793, 96
- Schlafly, E. F., et al. 2012, *ApJ*, 756, 158
- Schmidt, K. B., et al. 2016, *ApJ*, 818, 38
- Schneider, P., & Sluse, D. 2013, *A&A*, 559, A37
- Seitz, S., Saglia, R. P., Bender, R., Hopp, U., Belloni, P., & Ziegler, B. 1998, *MNRAS*, 298, 945
- Shibuya, T., Kashikawa, N., Ota, K., Iye, M., Ouchi, M., Furusawa, H., Shimasaku, K., & Hattori, T. 2012, *ApJ*, 752, 114
- Shibuya, T., Ouchi, M., & Harikane, Y. 2015, *ApJS*, 219, 15
- Sluse, D., Claeskens, J.-F., Hutsemékers, D., & Surdej, J. 2007, *A&A*, 468, 885
- Stark, D. P., Ellis, R. S., Richard, J., Kneib, J.-P., Smith, G. P., & Santos, M. R. 2007, *ApJ*, 663, 10
- Suyu, S. H., et al. 2013, *ApJ*, 766, 70
- . 2014, *ApJ*, 788, L35
- . 2016, *ArXiv e-prints*
- Tewes, M., et al. 2013, *A&A*, 556, A22
- Tonry, J. L., et al. 2012, *ApJ*, 750, 99
- Treyer, M., & Wambsganss, J. 2004, *A&A*, 416, 19
- Wong, K. C., et al. 2016, *ArXiv e-prints*
- Wright, E. L., et al. 2010, *AJ*, 140, 1868
- Xu, D., Sluse, D., Gao, L., Wang, J., Frenk, C., Mao, S., Schneider, P., & Springel, V. 2015, *MNRAS*, 447, 3189
- Yonehara, A. 2006, *ApJ*, 646, 16